Energy and structure of inertial range turbulence deduced from an evolution of fluid impulse

D. M. Summers
School of Mathematics and Statistics, Napier University, 10 Colinton Road, Edinburgh EH10 5DT, Scotland
(Received 7 February 2001; revised manuscript received 7 December 2001; published 5 March 2002)

We explore numerically a very simple idea that may provide a material explanation for inertial range turbulence. We base a Lagrangian model of viscous incompressible fluid flow on an evolving ensemble of vortex doublet sheets. Initially these are randomly oriented and randomly distributed within a disk in two-dimensional space. These sheets are then actively transported (in two dimensions) according to the Oseledets equation of motion for fluid impulse. The mutual interaction of these sheets, and their diffusion, establishes a velocity fluctuation field. In a specific sense this evolution is self-affine, and we exploit this property to calculate standard statistical measures for the fluctuation field. We determine from this simple model the second-order structure function and the energy spectrum of inertial range turbulence.

DOI: 10.1103/PhysRevE.65.036314 PACS number(s): 47.27.−i, 47.11.+j, 05.40.−a, 89.75.Da

I. INTRODUCTION

A complete mathematical theory of turbulence deduced from equations of motion has proved elusive. Although turbulence is observed to be, at small scale, a complex fluctuating velocity field, flow regimes characterized by the ''inertial range'' of turbulence appear to exhibit strikingly simple statistical properties. For example, one statistical measure (the second-order structure function) assumes in this regime a $r^{2/3}$ dependence (r being the separation between two correlation points). The 2/3 power-law exponent is consistent with the prediction—based on dimensional analysis—determined by Kolmogorov [1] and Obukhov [2]. The question of how such scale relationships arise from the equations of motion is a long-standing preoccupation of research in this area.

In an experimental setting, turbulence is typically generated by passing fluid over a solid surface. Turbulence generated at such boundaries becomes subsequently transported into the flow interior. The present paper is motivated by a speculative identification of such turbulence creation with the creation of fluid impulse at a solid boundary as described in Refs. [3–5]. In particular, a vortex doublet sheet is continuously created at a solid boundary in response to viscous boundary conditions. This sheet fragments and evolves through viscous diffusion and through advection (accompanied by rotation and stretching) into the flow interior according to the equation of motion introduced by Oseledets [6]. (The physical interpretation of this as an equation of motion for fluid impulse density was introduced by Buttke [7].) The elements of this developing ensemble of doublet fragments induce a local contribution to the velocity. This induced contribution is influenced by the fact that the trajectories of the inducing doublet fragments have, in part, a stochastic character: they constitute a system of advecting and diffusing submacroscopic sources. The effect of this is to establish, in ensemble, a velocity fluctuation field.

In the following, we give a brief Lagrangian account of this generation of impulse at a wall. The character of the fluctuation field that develops in the immediate neighborhood of the wall has been discussed elsewhere (see Ref. [5]). As time progresses the created elements of impulse evolve from the near-wall regime into the flow interior; in the present paper, we investigate numerically the statistical properties of the associated fluctuations in such an interior regime. To do this we conceive of an ensemble of doublet elements randomly distributed within a compact subdomain of unbounded space. The ensemble represents an unforced, decaying system. In the present paper, we explore this model for two-dimensional geometry. We calculate the two-point covariance of the resulting velocity fluctuation field at a particular instant during this evolution.

The foregoing material explanation of the process of turbulence differs in a fundamental way from that associated with the Kolmogorov-Obukhov theory [1,2] or with its elaboration for two dimensions described by Kraichnan [8] (see also Ref. [9] for a discussion of Batchelor's contribution to this subject). We do not conceive, explicitly, of a cascade process, nor do we invoke the limit of infinite Reynolds number (i.e., we do not associate inertial range turbulence with the zero-viscosity limit). In Sec. III D, we argue that the inertial range is characterized by the condition that—expressed in terms of the kinematics of impulse doublet sheets—diffusive displacement is comparable in magnitude to advective displacement. Thus, we are in a regime that is far from flow constrained by inviscid constants of motion. We will show that, in this regime, the kinematics satisfies a self-affine property and that it is this property that leads to the power-law exponents predicted by Kolmogorov.

The simple model we present here depends fundamentally on the Brownian motion of fragments of impulse density. Thus, we are describing a viscous mechanism. We recall the remark of Kraichnan [10] to the effect that the Kolmogorov-Obukhov power-law exponents are experimentally observed far from the high Reynolds number range of validity we usually associate with Kolmogorov theory. For example, note Figs. 5.7 or 5.8 in Frisch [11]. The present model can offer an explanation for this unexpectedly extensive spectral range of the power laws.

II. EVOLUTION OF IMPULSE

A representation of flow in terms of fluid impulse is achieved by postulating a simple ''constitutive relationship''

to accompany the momentum equation; this is, namely, a decomposition (first proposed by Kuz'min [12]) through which the velocity field of an incompressible fluid is expressed as the sum of a ''local field'' (which is the density of fluid impulse), and of a ''nonlocal field.'' This postulate is made in a manner analogous to the postulating of constitutive relationships to accompany Maxwell's equations in electromagnetism. Kuz'min's decomposition can be stated as

$$\mathbf{u}=\mathbf{m}+\operatorname{grad}\phi, \tag{2.1}$$

where $\mathbf{u}$ is velocity (with vanishing divergence); $\mathbf{m}$ is impulse density (whose curl and divergence are both nonvanishing); and ϕ is a scalar field (the curl of grad ϕ vanishes identically). The relationship (2.1) can be formally classed as a Hodge decomposition of $\mathbf{m}$, which is to say a decomposition into a solenoidal field $(\mathbf{u})$, and an irrotational field $(\operatorname{grad}\phi)$.

Oseledets [6] determined that if Eq. (2.1) is substituted into the Navier-Stokes equation (and if, as Russo and Smereka [13] observe, a particular choice of gauge is made) an equation of motion for $\mathbf{m}$ is obtained

$$D\mathbf{m}/Dt=-(\boldsymbol{\nabla}\mathbf{u})^{T}\mathbf{m}+\mathrm{Re}^{-1}\,\Delta\mathbf{m} \tag{2.2}$$

(with an accompanying decoupled equation for ϕ). Re is the Reynolds number. The operator D/Dt is the time derivative along particle trajectories; Δ is the Laplacian operator; and the ij element of the matrix $(\boldsymbol{\nabla}\mathbf{u})^{T}$ is $\partial u_j/\partial x_i$ for a velocity field $\mathbf{u}=(u_1,u_2,u_3)$ at a point (x_1,x_2,x_3) in three-dimensional space. The first term on the right hand side of Eq. (2.2) represents the deformation and rotation of a material element of the field $\mathbf{m}$ as it evolves in the stream. Our choice of gauge is made in order to achieve the separated Eq. (2.2) that we require for a Lagrangian model. This equation is consistent with a Hamiltonian form [6]; exploiting this fact, Buttke [7] and Buttke and Chorin [14] demonstrate that numerical models of inviscid three-dimensional fluid motion can be based on tracking elements of the impulse density variable $\mathbf{m}$ as these evolve in the flow. Lagrangian models based on impulse have been pursued in a number of inviscid contexts—for example, in the modeling of the motion of an immersed membrane [15,16]. We note too the model of inviscid turbulence developed by Smereka [17] that is based on the Euler form of Eq. (2.2).

Since we attach to $\mathbf{m}$ a material interpretation, Eq. (2.2) can be understood as an equation of motion for a field that has compact support, in fact analogous to the evolution of a source density field in a magnetic material. We conceive it to be comprised of an ensemble of vortex dipoles. We can understand the nonlocal field grad ϕ as a volume (or ensemble) weighted average of $\mathbf{m}$. The implication of Eq. (2.1) is that the two fields $\mathbf{m}$ and grad ϕ (which are, respectively, local and nonlocal) interpenetrate, and in summation, constitute the divergence-free velocity field $\mathbf{u}$.

To understand the physical origin of $\mathbf{m}$ we look to the boundaries of the flow. When a moving viscous fluid is in contact with a solid wall, we impose two boundary conditions there. The fact that the fluid does not penetrate the wall is expressed through an impermeability condition: the normal component of the velocity field vanishes at the boundary. Also, we consider the fluid to adhere at the wall, implying a no-slip condition there. These two conditions are expressed as the union on ∂D of

$$\mathbf{u}\cdot\mathbf{n}=0, \tag{2.3a}$$

$$\mathbf{u}\cdot\mathbf{s}=0, \tag{2.3b}$$

where $\mathbf{n}$ is a unit vector normal to ∂D and $\mathbf{s}$ is a unit vector tangential to ∂D. Substituting Eq. (2.1) into Eqs. (2.3), we infer the following conditions to be satisfied by $\mathbf{m}$ at the wall,

$$\mathbf{m}\cdot\mathbf{n}=-\partial\phi/\partial n, \tag{2.4a}$$

$$\mathbf{m}\cdot\mathbf{s}=-\partial\phi/\partial s. \tag{2.4b}$$

Identifying $\mathbf{m}$ as an impulse density has a natural significance at such a boundary. Impulse is a time integral of force taken in the limit of vanishing time interval. We will understand Eqs. (2.4) as relationships that express the impulse imparted to the flow at an instant of time, in response to an impinging velocity field whose potential is given by ϕ. We apply the divergence operator to Eq. (2.1) and noting that $\operatorname{div}\mathbf{u}=0$ for incompressible flow, we deduce the Poisson equation

$$\Delta\phi=-\operatorname{div}\mathbf{m}. \tag{2.5}$$

If we constrain impulse to be normal at the wall, the boundary condition (2.4b) implies the condition $\partial\phi/\partial s=0$ there. This condition ensures the existence of a solution (unique to an additive constant) to the differential equation (2.5); the vector grad ϕ is therefore uniquely determined and the Kuz'min decomposition (2.1) will also be uniquely determined for such a case. We refer now to the first equation in Eq. (2.4), namely, $\mathbf{m}\cdot\mathbf{n}=-\partial\phi/\partial n=-\mathbf{n}\cdot\operatorname{grad}\phi$. At a fixed time (t_o) we consider the boundary ∂D to lie outside the support of previously created impulse (i.e., created in $t<t_o$). We observe that if we can solve (2.5) to deduce grad ϕ, then we can proceed to calculate that normal impulse (imparted to the flow at ∂D) which is required to effect impermeability, i.e., we can calculate $\mathbf{m}$ there. The support of this created field will necessarily be that of a thin sheet coincident with the wall [it therefore does not contribute to the right hand side of Eq. (2.5) at $t=t_o$]. This field subsequently evolves from the wall into the fluid interior over the following time interval according to Eq. (2.2).

The impermeability condition need not occupy a privileged position: we can equally constrain impulse to be tangential at the wall. In this case the first equation in Eq. (2.4) implies the boundary condition $\partial\phi/\partial n=0$ on ∂D. The solution of Eq. (2.5), consistent with this condition, determines an alternative, and complementary function ϕ, with a vector function grad ϕ again uniquely determined. We deduce that the impulse on ∂D required to effect the no-slip condition is given by $\mathbf{m}\cdot\mathbf{s}=-\mathbf{s}\cdot\operatorname{grad}\phi$.

We have, in effect, decomposed the viscous boundary conditions into two complementary modes of impulse cre-

ation. In Refs. [3–5], we describe the mode that derives from $\partial\phi/\partial n=0$ on ∂D as ''Case I,'' and that which derives from $\partial\phi/\partial s=0$ on ∂D as ''Case II.'' Both these modes can occur in superposition (see Sec. 4.2 in Ref. [5]). Once created, such impulse evolves from the wall into the flow interior according to the transport equation (2.2). We can represent this process as the creation, at successive instants of time, of an assembly of impulse dipoles at the wall. In both cases we can appeal to the electromagnetic analogy to understand their physical significance (see, for example Ref. [4]). Dipoles created normal at the wall are equivalent to a system of vortex loops coincident with the surface. In the near-wall regime these elements are closely related to the separation or attachment of flow. In two dimensions this distribution of dipoles constitutes a vortex singlet sheet. As these created objects evolve from the wall they represent, in ensemble average, the developing flow topology.

Dipoles created tangential at the wall are, upon ensemble average, equivalent to a vortex doublet sheet. In the context of inertial range problems, we conceive of this sheet (and its partitions) as retaining thin-sheet character during subsequent evolution. As such a sheet disintegrates due to viscous diffusion, the resulting fragments retain their identity as doublet sheets, irrespective of their spatial scale. The evolution of an ensemble of such fragments has a distinct self-affine property (described in Sec. IV B below). We associate this ensemble with the submacroscopic fluctuation field of a fluid.

III. SOURCE OF VELOCITY FLUCTUATION

A. Unbounded ensemble of doublet sheets

We have explained that tangential impulse created at a boundary ∂D, taken in ensemble, can be considered to be a vortex doublet sheet coincident with the wall. This sheet will be subject to diffusive transport, a process that can be modeled numerically by partitioning the doublet sheet into an assembly of contiguous patches each characterized by spatial length scale λ. The parameter λ may be chosen to reflect a ''roughness length'' of the originating surface, or in the case of a smooth surface, it may be rationally chosen to be of order Re^{-1} (see Ref. [3]). The segments subsequently form a growing ensemble of elements embedded in the flow interior. These constitute an N-body problem governed by a dipole-dipole interaction field. The interaction of a system of sheets arbitrarily oriented with respect to each other can be expressed by coordinate rotations in space. Each element of the ensemble moves in the velocity field collectively induced by the remaining $N-1$ other elements. The elements continue to be subjected to viscous diffusion in the flow interior; the ensemble is thus dissipating (and is without external forcing).

The ensemble of interacting elements reflects the nonlinear character of fluid flow. As each element moves in the field induced collectively by the ensemble, its own position relative to this ensemble changes; the dipolar interaction field (as measured at a fixed point) which is contributed to the flow by a particular element, evolves over time. Over the time, an evolving fluctuation field at this point can be formed by establishing the difference between the instantaneous field and the evolving mean field at the point.

In the present paper, we ascertain whether an ensemble of such doublet sheets can give rise to a flow with the same statistical signature as that found in physical turbulence experiments. We confine our attention to two specific statistical measures of inertial range turbulence (which is to propose to model a spatially unbounded flow that is statistically stationary and isotropic, and for which the fluctuation intensity is low relative to the mean velocity field). We do this by means of a simple two-dimensional model. We distribute N impulse doublet sheets randomly within a disk of radius R; each sheet has uniform length λ, but is randomly oriented. (Lengths are reckoned in dimensionless units.)

B. A "correlation probe"

In order to characterize the fluctuation statistics of the resulting flow, we design a ''numerical probe'' consisting of an $n\times n$ square array of measurement locations that is to be situated within a square with sides of length L. This probe is to be placed at an arbitrary position within the ensemble disk.

At each of these n^2 ''subprobe'' array locations (denoted by the position vector $\mathbf{r}$) we measure, at a particular time step, the velocity fluctuation $\mathbf{u}'(\mathbf{r})$, relative to the local mean field $\mathbf{U}(\mathbf{r})$ (which we calculate as an accumulating mean over preceding steps). Each pairwise nonrepeating combination of locations is considered in turn, establishing an ensemble of $\frac{1}{2}n^2(n^2+1)$ evaluations of a two-point spatial correlation $\mathbf{u}'(\mathbf{r})\cdot\mathbf{u}'(\mathbf{r}+\boldsymbol{\rho})$. We consider the fluctuation components projected onto the direction of the separation vector $\boldsymbol{\rho}$ to form a longitudinal component of fluctuation $\mathbf{u}'_{\parallel}$, and onto a direction orthogonal to this, to form a transverse component $\mathbf{u}'_{\perp}$. We sort these in ascending value of the separation variable $\rho=|\boldsymbol{\rho}|$, and an ensemble average is formed from these to determine longitudinal and transverse covariance functions defined by

$$\Gamma_{\parallel}(\rho)=\langle\mathbf{u}'_{\parallel}(\mathbf{r})\cdot\mathbf{u}'_{\parallel}(\mathbf{r}+\boldsymbol{\rho})\rangle$$

and

$$\Gamma_{\perp}(\rho)=\langle\mathbf{u}'_{\perp}(\mathbf{r})\cdot\mathbf{u}'_{\perp}(\mathbf{r}+\boldsymbol{\rho})\rangle.$$

The symbols $\langle\ \rangle$ denote spatial ensemble average, i.e., for a discrete set of P evaluations $\{\mathbf{a}^{(j)}\}$ of a continuum field we would define

$$\langle\mathbf{a}\rangle=\lim_{P\to\infty}\frac{1}{P}\sum_{j=1}^{P}\mathbf{a}^{(j)}.$$

In the context of numerical or physical measurements, this average is approximated by truncation.

Here, we have assumed isotropy in the flow, i.e., cross covariance is neglected. The validity of this assumption can

be examined by evaluating the corresponding cross covariance function defined by

$$\Gamma_{\text{cross}}(\rho)=\langle \mathbf{u}'_{\perp}(\mathbf{r})\cdot\mathbf{u}'_{\parallel}(\mathbf{r}+\boldsymbol{\rho})+\mathbf{u}'_{\parallel}(\mathbf{r})\cdot\mathbf{u}'_{\perp}(\mathbf{r}+\boldsymbol{\rho})\rangle.$$

C. Energy and structure

The energy spectrum to be associated with a three-dimensional flow can be calculated from the three-dimensional Fourier transform of the covariance $\Gamma(\rho)$. By virtue of the isotropy of the model, this transform simplifies to

$$E(K)=\frac{1}{\pi}\int_0^\infty \rho K\Gamma(\rho)\sin K\rho d\rho, \tag{3.1}$$

where K represents wave number. Equation (3.1) is a manifestation of the Wiener-Khinchin relationship.

The second-order longitudinal structure function $S_2(\rho)$ is formed by calculating at each probe location the product $[\mathbf{u}'(\mathbf{r})-\mathbf{u}'(\mathbf{r}+\boldsymbol{\rho})]\cdot\hat{\boldsymbol{\rho}}$, where $\hat{\boldsymbol{\rho}}$ is the unit vector in the separation direction; this quantity is squared and then ensemble averaged. A similar calculation can be carried out for the transverse case.

In the particular circumstances that we have described (i.e., isotropy, stationarity, low fluctuation intensity, etc.) physical experiment shows that there exist particular ranges of the independent variables ρ and K for which the functions $S_2(\rho)$ and $E(K)$ exhibit simple power-law relationships. Specifically, there can exist a range of ρ for which

$$S_2(\rho)\propto\rho^{2/3} \tag{3.2}$$

and a range of K such that

$$E(K)\propto K^{-5/3}. \tag{3.3}$$

The indices ''2/3'' and ''$-5/3$'' are often described as the Kolmogorov-Obukhov [1,2] exponents. Obukhov demonstrated that the relationship (3.3) is consistent with Eq. (3.2)—see also chap. 4 of Frisch [11]. The regime implied by these power-law relationships is the ''inertial range'' of turbulence. The evidence of these simple dependences across a variety of phenomena of varying scale and context, is consistent with a view that these ranges are, in a specific sense, ''universal'' (see Fig. 2.4 in Ref. [18]).

D. Kinematical definition of inertial range

A Reynolds number appropriate to turbulence measurements can be defined as

$$\text{Re}=\ell_o\langle u'^2\rangle^{1/2}/\nu \tag{3.4}$$

where the reference length ℓ_o represents the upper spatial scale of eddies in the inertial range; $\langle u'^2\rangle^{1/2}$ represents the rms value of velocity fluctuation; and ν is kinematic viscosity (this is discussed, for example, in Sec. 7.3 of Ref. [11]).

In the present paper, we are considering an evolving ensemble of doublet sheet elements each ''carrying'' a length dimension. (The ith element will have a length denoted as λ_i.) In the context of real flows the elements of $\{\lambda_i\}$ may derive from an originating surface characterized by a spatial spectrum of roughness scales. Moreover a sheet fragment typically becomes stretched in the stream, and it can fold, implying an evolution in scale. Therefore, we can expect an interior ensemble of doublet sheets to consist in a variety of length scales.

Our object is to fashion within such a Lagrangian construction the conditions of inertial range turbulence. We understand this, in kinematical terms, to be a flow regime in which diffusive displacements and inertial displacements of a doublet element are comparable in magnitude (over a common time interval dt). Consider an element of length λ: a regime where such displacements are comparable can be determined by equating a stochastic displacement $\eta=\sqrt{2dt/\text{Re}}$ (which models viscous diffusion through random walks) to the advective displacement determined by Eqs. (22) and (23) in Ref. [3]. This leads to the relationship between Reynolds number and sheet length parameter reported in Ref. [3], namely,

$$\text{Re}\sim O(\lambda^{-1}). \tag{3.5}$$

The flow regime characterized in this way lies at a transition between flow in which viscous diffusion dominates the kinematics, and one in which inertial forces dominate. We appreciate from Eq. (3.5) that the Reynolds number we associate with this transition (and consequently the associated diffusivity) is scale dependent.

We can attach to λ the role of reference length in the definition of Reynolds number. Thus in the case of an ensemble of uniform scale, we consider $\lambda=\ell_o$ to correspond to a representative eddy scale. We infer from Eqs. (3.4) and (3.5) that

$$\langle u'^2\rangle^{1/2}\sim O\left(\frac{\nu}{\lambda^2}\right) \tag{3.6}$$

at the transitional flow regime. To understand this relationship, let us conceive of a flow with a broad range of velocity fluctuations. Some of these may vary slowly so we can characterize these variations as nonstochastic in appearance. (We assume these will not contribute to correlation statistics.) Alternatively, some fluctuations will be of sufficiently high frequency, that they are submerged in a background of purely diffusive fluctuations. They contribute uncorrelated random noise to a measurement of covariance. We identify the range of fluctuations consistent with Eq. (3.6) as precisely the range that contributes to the covariance for a prescribed eddy scale λ.

Consider a doublet ensemble characterized by the presence of two scales λ_1 and λ_2. We associate with each scale a distinct transition regime, and a corresponding Reynolds number. If we consider these two subensembles to interpenetrate and consider that each constituent subensemble is engaged in a statistically independent stochastic process (i.e., with distinct Reynolds number), then the covariance of the composite ensemble can be developed from the ensemble average of the two constituent covariances. In the following, we will generalize this approach to embrace correlation for the discrete spectrum of scales $\{\lambda_i\}$.

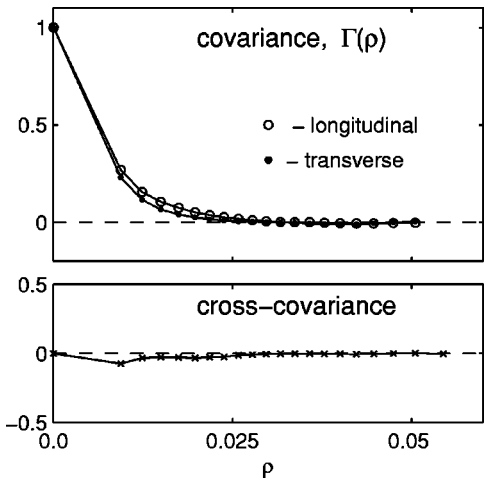

FIG. 1. Sample-averaged covariance functions for a single scale $\lambda = 0.002$; the corresponding cross covariance is illustrated below.

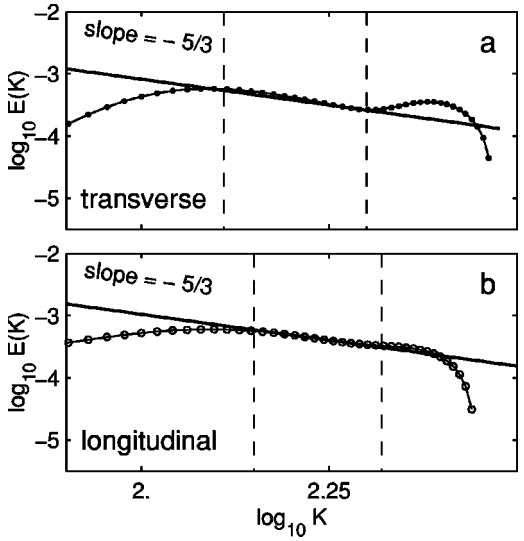

FIG. 2. Doubly logarithmic plot of energy spectra calculated from $\Gamma(\rho)$ shown in Fig. 1. These spectra relate to an ensemble consisting of only a single scale, $\lambda = 0.002$.

IV. NUMERICAL RESULTS: ENERGY SPECTRUM

A. Spectrum for single scale

To make a numerical demonstration of the foregoing account of turbulence statistics, we consider a disk of radius $R = 0.2$; we prescribe a Reynolds number $\mathrm{Re} = 500$, which determines a sheet segment length $\lambda = 0.002 \sim O(1/\mathrm{Re})$. In effect this specifies a lower bound to the spatial scale that can be resolved in the present exercise. We hence define an array of probe locations with a minimum separation of order λ: we consider 45×45 locations within a square of side $L = 0.06$. We place replicas of this probe at ten locations in the disk. Into this disk we introduce a distribution of $N = 1000$ sheet segments that are randomly positioned, and each has random orientation. This ensemble is allowed to interact with itself; it is also subject to viscous diffusion, modeled numerically using a random-walk representation. We allow this ensemble of elements to evolve for ten steps to establish a mean flow field through temporal average. (The present choice of N leads to a fluctuation intensity of about 10%.)

Each probe array gives rise to 2 049 300 evaluations of the correlation $\mathbf{u}'(\mathbf{r}) \cdot \mathbf{u}'(\mathbf{r}+\boldsymbol{\rho})$. These are sorted into 20 nonuniformly spaced class intervals of ρ values; the widths of these intervals are chosen so that there are an equal number of evaluations represented in each. An ensemble average is taken over each interval to develop the four functions $\Gamma_{\parallel}(\rho)$, $\Gamma_{\perp}(\rho)$, $\Gamma_{\mathrm{cross}}(\rho)$, and $S_2(\rho)$. These are, in turn, sample averaged over the ten probe locations in the flow. The class intervals for this example imply that $\rho_{\min} = 0.003$ and $\rho_{\max} = 0.05$. This bandwidth determines the corresponding range of K values to be determined through Eq. (3.1). We expect this range to fall in the interval $10 < K < 1000$.

Figure 1 illustrates the covariances for this numerical calculation, averaged over the ten location samples. (These covariance curves can be compared to experimental measurements, for example see Figs. 5.12 and 5.13 in Ref. [19].) The lower plot in Fig. 1 illustrates the associated cross covariance.

The energy spectra $E(K)$ associated with the covariances of Fig. 1 are illustrated in the log-log plot of Fig. 2; these are determined by applying a simple numerical quadrature (trapezium rule for nonequispaced partition) to a truncated version of the integral (3.1). The K regimes for both transverse and longitudinal spectra for which the gradient approximates the value ''$-5/3$'' are indicated by vertical dashed lines.

The appearance of regimes characterized by these linear gradients is typical of a range of numerical parameters, which is to say the linear regime of the energy spectra in log-log coordinates is typical. One has to ensure, however, that the prescription of probe parameters L and n are such that $\lambda \sim O(Ln^{-1})$ in order to achieve significant correlation. Also, the choice of ensemble size N and radius R (and hence particle density) should be made so that the fluctuation intensity is less than 10%.

We note the spectra in Fig. 2 conform to a power-law structure only over a relatively small interval in the neighborhood of $\log_{10} K \simeq 2.25$. The doublet ensemble we are considering in this example is ''monochrome,'' i.e., it consists of a single spatial scale λ. In physically measured flows such a uniformity of eddy scale is very unlikely to exist. The model of inertial range turbulence that underlies Kolmogorov scaling analysis is that of an ensemble of eddies of differing scale, extending from a maximum (the integral scale) down to a minimum (dissipation scale). To understand the covariance associated with a spatial range of scales, we now generalize the present single-scale model to embrace a discrete spectrum.

B. Self-affinity

An advantage of having developed the present particle model of ''turbulence'' is that it allows us to investigate how such a model scales with refined model resolution. We can construct a hierarchy of self-similar models of successively smaller scale and understand from the kinematics of this the underlying scaling properties. If all lengths (including the segment length λ) are linearly transformed by a common

scale factor, we arrive at a spatially scaled replica of our original doublet ensemble. Furthermore, if we scale time by this same factor, the advective kinematics will itself be a scaled replica of the original advection. Finally, if we impose $\mathrm{Re}\sim O(\lambda^{-1})$, the scaling of λ implies an inverse scaling of Re. The resulting random-walk displacements η with which we model viscous diffusion, will constitute a scaled replica of the original diffusion model.

We might expect from all this that $\Gamma(\rho)$ determined from the scaled numerical experiment will replicate at smaller scale the covariance function determined from the ''full-scale'' experiment, i.e., if ρ, λ, L, R, etc., are scaled by a factor k (such that $k<1$) so that $\rho'=k\rho$, we might expect $\Gamma(\rho)$ to be in some sense self-similar to $\Gamma(\rho')$. We recall von Kármán and Howarth's [20] analysis of the decay of isotropic turbulence, in which they make the assumption that the correlation function preserves its shape under spatial scaling. On the basis of the present discussion, we suggest this assumption finds a rational justification in the kinematics of impulse. Note that whereas the independent variable ρ is scaled (and the entire spatial model and its kinematics are strictly self-similar under this scaling), the statistical covariance function $\Gamma(\rho)$ continues to span the interval $[0,1]$ for all ρ at all scales. This reflects the multifractal nature of fluid turbulence, which has been described by Mandelbrot [21]. We characterize the relationship between the statistical measures relating to such scaled models as that of ''self-affinity.''

C. Hierarchy of scales

In Sec. IV A, we considered an ensemble characterized by a single scale ($\lambda=0.002$). This choice was arbitrary and similar results would be obtained for any choice of λ. In the case of an ensemble consisting of two ''subensembles'' ($\lambda=\lambda_1$, and $\lambda=\lambda_2$, respectively), we define a covariance by assuming that the fluctuations derived from the scaled numerical experiments described in Sec. IV B are statistically independent of each other. This derives from the fact that, although their kinematics are self-affine, the time scale and the diffusion coefficients of the scaled processes are nevertheless distinct. The covariance is formed by an ensemble-averaging exercise over all scales present; by virtue of the statistical independence, we organize this summation process into two parts: we separately form the covariance associated with λ_1 (denoting this as Γ_1) and then form that for λ_2 (denoted Γ_2). We hence form the ensemble average over these two contributions: namely, we form $\langle\Gamma(\rho)\rangle=\frac{1}{2}[\Gamma_1(\rho)+\Gamma_2(\rho)]$. In effect, we are forming the ensemble average of two ensemble averages. As a measurement exercise, we could adjust the parameter L of the correlation probe to determine in turn Γ_1 and Γ_2. Alternatively, we exploit the self-affinity implied by the kinematics and conceive of Γ_2 as a scaled image of Γ_1.

The foregoing strategy can be generalized in an obvious way. We consider a fluid to consist of a discrete spectrum of scales, such that this is captured by a range of probe dimensions in the interval $[L_{min},L_{max}]$. Consider an ensemble consisting of n interpenetrating ''subensembles,'' and consider specifically the interval between $\rho=0.006$ and $\rho=0.06$. We partition this into two equally spaced subintervals and construct from this three covariance functions encompassing the ρ domains: $\rho\in[0,0.006]$, $\rho\in[0,0.033]$, and $\rho\in[0,0.06]$. Each subinterval can again be bisected to determine two further subintervals, and from this, a total of five covariance functions can be constructed. The procedure can be repeated to determine successively nine functions, seventeen functions, etc. After j such successive bisections we determine a self-affine hierarchy of 2^j+1 functions. Figure 3 illustrates the case of 17 covariance functions (for the longitudinal case) determined in this way. These covariances are generated by assuming they are self-affine to the calculated $\Gamma(\rho)$ determined from the numerical probe for the interval $\rho\in[0.0,0.06]$, this case serving as a ''template.'' The thick solid line represents the ensemble average of these 17 curves, namely,

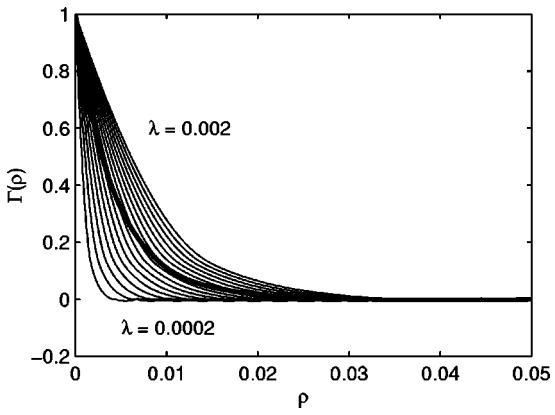

FIG. 3. Ensemble-averaged covariance (thick solid line) determined from a family of 17 scales.

$$\langle\Gamma(\rho)\rangle=\frac{1}{17}\sum_{j=1}^{17}\Gamma_j(\rho).$$

We pursue this exercise for $j=9$ successive bisections (bounded by $\rho\in[0,0.0001]$ and $\rho\in[0,0.06]$) and substitute the resulting ensemble-averaged covariance (averaged over a hierarchy of 513 scales) into the transform (3.1) to obtain the energy spectrum illustrated in Fig. 4. The linear regression formed on the interval $\log_{10}K\in[2.9,3.9]$ has a slope of -1.66 ± 0.06 that we offer as an encouraging approximation to the Kolmogorov-Obukhov exponent. We note the ''Spanish moss'' effect beyond the K range corresponding to the interval of averaging in Fig. 4; the phenomenon is discussed in a more general context on page 75 of Ref. [21]. Note also that as the foregoing bisection process is repeated for increasingly large j, we approach, in a pointwise sense, the condition of scale continuum.

V. NUMERICAL RESULTS: SECOND-ORDER STRUCTURE FUNCTION

A. Two scales in isolation

The numerical probe described in Sec. III A can be used to determine numerically the structure functions for the ensembles described in Secs. IV A and IV B. Figure 5 illus-

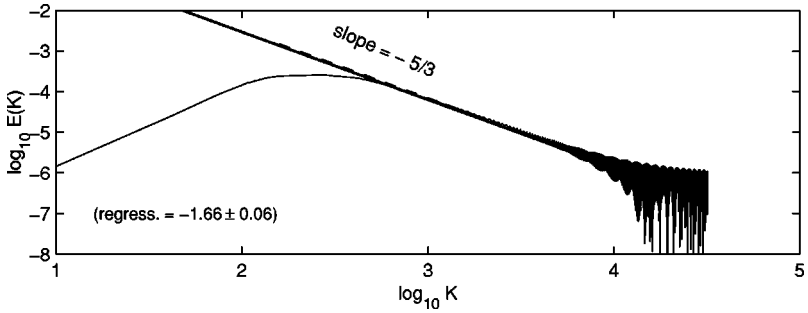

FIG. 4. Energy spectrum determined from the ensemble average of a family of 513 scales ($j=9$).

trates (in log-log format) the longitudinal (○) and transverse (●) second-order structure function for these respective scales taken in isolation. One notes that as ρ approaches its lower spatial bound (i.e., λ), $\Gamma(\rho)$ appears to conform asymptotically to a power-law exponent of "4/3," which is indicated for each curve in Fig. 5. We note that, as in the case of the energy spectrum illustrated in Fig. 2, the region over which a linear power-law exponent can be determined is relatively small; this again relates to the fact that we are considering two models in each of which a single scale is considered in isolation, i.e., we are considering two isolated ensembles each with uniform scale. We generalize this situation in the following section.

B. Hierarchy of scales

For a given λ, there is, in the present method, a numerical lower limit to the value of ρ for which we can estimate $S_2(\rho)$, namely, the scale of the sheet segment itself. It is therefore difficult to understand unambiguously the asymptotic structure of $S_2(\rho)$ for vanishing ρ. To generalize the present procedure to include an ensemble average over a family of scales (as discussed in Sec. IV C for the case of covariance) we need to impose on this problem some understanding of this point. We make the assumption that the structure associated with very small scales (relative to λ) is not affected by the structure at a large scale relative to λ. In practical terms, we extrapolate the structure function curve (for fixed λ) until its intersection point with the ρ axis (the point ρ_o say), and for $\rho<\rho_o$ we take $S_2(\rho)$ to be zero for this scale. On this basis we exploit self-affinity to extend the range of ρ for which we can describe a structure function.

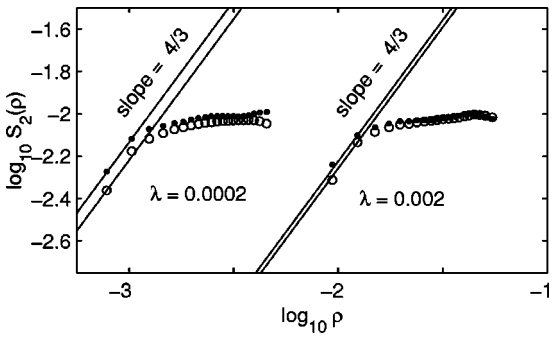

FIG. 5. Second-order structure functions for the transverse (●) and longitudinal (○) cases, for two individual scales each taken in isolation, $\lambda=0.0002$ and $\lambda=0.002$, respectively.

We consider a family of subscales ($\rho\in[0,0.006]$, $\rho\in[0,0.0033]$, etc.) and from this form a sequence, $S_2^{(1)}(\rho)S_2^{(2)}(\rho)$, etc. We hence calculate the ensemble average $\langle S_2(\rho)\rangle$. Figure 6(a) illustrates a family of functions corresponding to a self-affine hierarchy of scales; the solid thick line is the ensemble average of this hierarchy. This average is plotted in log-log coordinates in Fig. 6(b), with the 2/3 linear slope indicated. For ρ approaching the lower limit of scales represented in the ensemble, the 4/3 slope is also indicated.

It is interesting to note that we can attach some physical significance to the maximum point of intersection of $S_2(\rho)$ with the ρ axis in the family of curves illustrated in Fig. 6(a). Let us characterize this value of ρ_o as the maximum eddy size λ_0, in the ensemble, and write $\lambda_o=\max\{\rho_o\}$. Figure 6(b) illustrates how the parameter λ_0 delimits a lower bound to

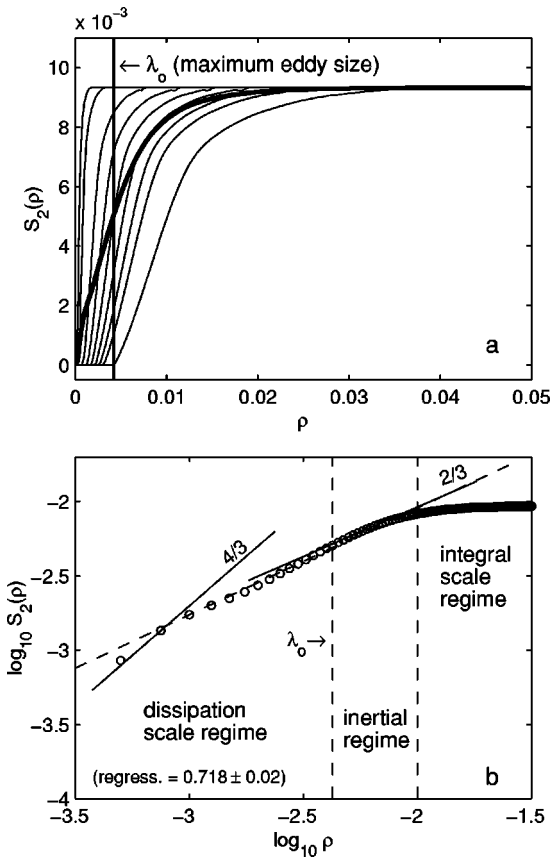

FIG. 6. (a) Structure functions associated with a family of scales, and their ensemble average (thick solid line); and (b) doubly logarithmic plot of the latter average.

the scale of inertial range turbulence, i.e., a regime approximated by a 2/3 power-law exponent consistent with that determined by Kolmogorov. We also indicate in Fig. 6(b) the integral scale regime, and the dissipation scale regime consistent with this interpretation of λ_0. Note that in the inviscid limit, the scaling described in Sec. III D implies the delimiting line labeled λ_0 in Fig. 6(b) will proceed to the left of the diagram. As the inviscid limit is approached, the inertial regime is extended towards smaller scales.

The sloping dashed line in Fig. 6(b) represents the linear regression in the interval $\log_{10}\rho\in[-3.0,-2.0]$, which has a slope of 0.718 ± 0.02. It is interesting to note that this latter value approximates the value of 0.7 for the power-law exponent that has been determined experimentally by a number of authors—for example, see Fig. 3 of Ref. [22]. In this context it is relevant to note a comment of Viecelli [23]. He remarks that if an intermittency correction (as developed in chap. N15 of Ref. [21]) is applied to a Lagrangian structure function determined from a 4/3 scaling law (i.e., a Richardson law), then the power-law exponent for $S_2(\rho)$ can be determined to be 0.72. We emphasize that the calculations leading to Fig. 6(b) do not derive from such a prescribed scaling law (i.e., we do not impose a model of superdiffusivity onto the kinematics). Rather, the power-law exponents we calculate derive from the scaling properties (and presumably the intermittency) intrinsic to a simple Lagrangian representation of the equation of motion Eq. (2.2) in which viscous diffusion is modeled, in a standard way, through normally distributed Brownian motions.

VI. CONCLUSIONS

We offer here a simple constitutive (or material) answer to what has been an enduring question: how is turbulence related to the equations of motion? Our answer is one that both explains the physical origin of turbulence at a wall, and which accounts for the appearance of two power-law signatures in experimental measurements of velocity fluctuation. We demonstrate this by means of computational experiments that exploit the ensemble kinematics of doublet sheet elements.

The notion that a surface of material discontinuity in a viscous flow constitutes a generator for fluid impulse is not a phenomenological hypothesis as such. Rather, it derives in a simple way from the implication of force equilibrium at an interface. An ensemble of created doublets (in the absence of viscosity) is a discrete Hamiltonian system. Our conjecture is that the material substructure also of viscous flow is represented by such an ensemble and that Kuz'min's decomposition Eq. (2.1) is the constitutive relationship that discloses this structure. (This conjecture is not new: it is essentially that which animates the discussion in Refs. [14,24].)

A fluid may consist of a range of characteristic eddy scales, and we explore this by introducing a numerical probe that ''measures'' the covariance for a scale determined by the minimum separation of probe sublocations. The covariance associated with a variety of scales can be constructed through an ensemble average over the covariances associated with the constituent scales. We choose model and flow parameters such that the constituents of this average form a self-affine hierarchy of statistically independent random processes in the neighborhood of a kinematical version of the inertial range. With this procedure we determine an approximation to the Kolmogorov-Obukhov exponents.

In developing the energy power-law spectrum illustrated in Fig. 4, we have not invoked the limit of vanishing viscosity, i.e., we have not considered the limit $\nu\rightarrow0$. The ''$-5/3$'' energy exponent is consistent with that determined by Kolmogorov [1] and Obukhov [2] (but note also that neither of these authors invokes the limit $\nu\rightarrow0$). This spectrum also corresponds to that which is widely measured experimentally. On the other hand, an exclusively ''$-5/3$'' exponent is not consistent with the energy spectrum determined by Kraichnan [8] for two-dimensional flow. The latter result depends on imposing inviscid flow constraints, which is to say it depends on the zero-viscosity limit. These constraints are, namely, the constancy of energy implying the spectral condition

$$\int_0^\infty E(K)dK=\text{const}$$

and the constancy of enstrophy along stream lines implying

$$\int_0^\infty K^2E(K)dK=\text{const.}$$

The results of this latter analysis are widely taken as evidence that such two-dimensional models cannot represent the observed energy spectrum of real three-dimensional turbulence. In the context of our alternative impulse-based model, we suggest the present two-dimensional model does in fact approximate the energy spectrum observed in three-dimensional turbulence.

The notion that incompressible viscous fluid consists, in part, of an interpenetrating ensemble of doublet vortex elements derives from the understanding of the interaction of a viscous fluid with a boundary that is described in Ref. [5]. After ''long time'' has elapsed, such elements may eventually lose deterministic memory of the conditions of their creation. The spatial scale and orientation of an individual element will evolve along with its position according to Eq. (2.2); it will be subjected to a regime of stretching and diffusion. However, what will be preserved in this process, is the dipolar structure of the compactly supported impulse density field. It is not clear whether this local dipolar contribution to the flow is expressed in the solution to a randomly-forced Navier-Stokes equation when this problem is posed in two-dimensional unbounded space. Since we want to attach to an impulse doublet sheet the significance of a physical dipole source, we probably require either to describe the creation of these dipoles (through a time-evolutionary boundary value problem, say) or to postulate their existence (in a statement of initial data, for example). This is to emphasize that, in incompressible flow, we conceive turbulence to originate at a boundary.

The Hodge decomposition expressed in Eq. (2.1) reflects a mathematical property of solenoidal fields, in general. We

infer from this that the decomposition (i.e., into local and nonlocal constituents) which is made explicit in the impulse formulation, will be implicit in the evolution of momentum or vorticity. In the present paper, we hypothesize that turbulence results from the imparting of impulse into a viscous flow at a boundary. For this reason the impulse formulation of the problem has a natural advantage for us, not only in the equation of motion, but also in the direct way in which the boundary conditions can be expressed. However it may also be possible to cast the present model of impulse creation in terms of primitive variables or in terms of vorticity. To do this we would require boundary conditions for primitive variables (specifically for the pressure) and for vorticity that correspond to our treatment of the conditions for ϕ described in Sec. II. We suggest such conditions for pressure and vorticity could reasonably be characterized as ''natural conditions'' in the sense they would derive from the implications of Newton's third law at a boundary.

The Lagrangian impulse sheet formulation may provide further physical insight into the relationship between Newton's laws and the phenomenology of turbulence. For example, we note in Sec. III D that, given an ensemble of doublet sheets with uniform length scale λ, the Reynolds number to be associated with transition from flow dominated by diffusion, to flow dominated by advection, is given by $\mathrm{Re}\sim O(\lambda^{-1})$. Moreover in Sec. IV B, we note the scaling of Reynolds number that ensures the kinematical self-affinity of viscous flow across a range of scales is also given by $\mathrm{Re}\sim O(\lambda^{-1})$. We suggest that it is the conjunction of these two facts that determines the scaling properties of inertial range turbulence.

The numerical evidence of the present paper may make some contribution to a continuing debate about the role of viscosity in turbulence. Opinion divides on whether the properties of turbulent flow derive fundamentally from inviscid dynamics or otherwise—see Ref. [25].

We note that when we sum over a scale hierarchy, we are summing over particle models each characterized by a ''scaled'' Reynolds number. This recalls the argument of Barenblatt *et al.* [26] that the proportionality factors in Eqs. (3.2) or (3.3) are Reynolds number dependent if Re is sufficiently removed from its inviscid asymptote. In the context of the present Lagrangian model, any characterization of a system of interpenetrating ensembles of differing scale by a *single* Reynolds number will at best serve to approximate the condition of strict self-affinity. The quality of this approximation may improve in the limit of vanishing viscosity; it should be possible to exploit the present model to investigate this conjecture numerically.

We accept that some aspects of turbulence phenomena may require a more ambitious three-dimensional treatment, as well as requiring time differentiation of turbulence measures. To relate the present material model to the accepted theories of turbulence (e.g., the theory of Kolmogorov [1] or its elaboration by Kraichnan [8] and others), the present model should be pursued into the limit of vanishing viscosity. The underlying model can be naturally refined for this purpose, and generalized into three dimensions (see Refs. [27,28]).

[1] A.N. Kolmogorov, Dokl. Acad. Nauk SSSR **30**, 299 (1941) [English translation in *Selected Works of A.N. Kolmogorov*, edited by V.M. Tikhomirov (Kluwer Academic, Dordrecht, 1991)], Vol. 1.

[2] A.M. Obukhov, Dokl. Akad. Nauk SSSR **32**, 22 (1941).

[3] D.M. Summers, J. Comput. Phys. **158**, 28 (2000).

[4] D.M. Summers, Proc. R. Soc. London, Ser. A **456**, 1183 (2000).

[5] D.M. Summers, Physica D **154**, 287 (2001).

[6] V.I. Oseledets, Russ. Math. Surveys **44**, 210 (1989).

[7] T.F. Buttke, in *Vortex Flows and Related Numerical Methods*, Vol. 395 of *NATO Advanced Study Institute, Series C*, edited by J.T. Beale, G.-H. Cottet, and S. Huberson (Kluwer Academic, Dordrect, 1993), pp. 301–306.

[8] R.H. Kraichnan, Phys. Fluids **10**, 1417 (1967).

[9] G.I. Barenblatt, Not. Am. Math. Soc. **48**, 800 (2001).

[10] R.H. Kraichnan, J. Fluid Mech. **62**, 305 (1974).

[11] U. Frisch, *Turbulence—The Legacy of A. N. Kolmogorov* (Cambridge University Press, Cambridge, U.K., 1995).

[12] G.A. Kuz'min, Phys. Lett. **96A**, 88 (1983).

[13] G. Russo and P. Smereka, J. Fluid Mech. **391**, 189 (1999).

[14] T.F. Buttke, and A.J. Chorin, Appl. Numer. Math. **112**, 47 (1993).

[15] R. Cortez, J. Comput. Phys. **123**, 341 (1996).

[16] R. Cortez and D.A. Varela, J. Comput. Phys. **138**, 224 (1997).

[17] P. Smereka, Nonlinearity **9**, 1361 (1996).

[18] W.D. McComb, *The Physics of Fluid Turbulence* (Oxford University Press, New York, 1991).

[19] M.T. Landahl, and E. Mollo-Christensen, *Turbulence and Random Processes in Fluid Mechanics* (Cambridge University Press, Cambridge, U.K., 1986).

[20] T. von Kármán and L. Howarth, Proc. R. Soc. London, Ser. A **164**, 192 (1938).

[21] B. Mandelbrot, *Multifractals and 1/f Noise* (Springer-Verlag, Berlin, 1999), pp. 389–415.

[22] R. Benzi, S. Ciliberto, C. Baudet, and G.R. Chavarria, Physica D **80**, 385 (1995).

[23] J.A. Viecelli, Phys. Fluids A **1**, 1836 (1989).

[24] A.J. Chorin, *Vorticity and Turbulence* (Springer-Verlag, Berlin, 1994).

[25] A.J. Chorin, in *The Collected Works of Lars Onsager*, edited by P.C. Hemmer *et al.* (World Scientific, Singapore, 1996).

[26] G.I. Barenblatt, A.J. Chorin, and V.M. Prostokishin, Physica D **127**, 105 (1999).

[27] D.M. Summers, and A.J. Chorin, in *Vortex Flows and Related Numerical Methods II*, Vol. 1 of *Proceeding of the European Series in Applied and Industrial Mathematics*, edited by Y. Gagnon, G.-H. Cottet, D.G. Dritschel, A.F. Ghoniem, and E. Meiburg (unpublished), pp. 65–76 (http://www.emath.fr/Maths/Proc/Vol.1).

[28] D.M. Summers, and A.J. Chorin, Proc. Natl. Acad. Sci. U.S.A. **93**, 1881 (1996).